Multiwavelength generation from multi-nonlinear optical process in a 2D PPLT

Zohra Yellas, Min Won Lee, Régis Kremer, Kai-Hsun Chang, Mahmoud R. Beghoul, Lung-Han Peng, Azzedine Boudrioua

Multiwavelength generation from multi-nonlinear optical process in a 2D PPLT

ZOHRA YELLAS,[1] MIN WON LEE,[2,*] RÉGIS KREMER,[3] KAI-HSUN CHANG,[4] MAHMOUD R. BEGHOUL,[1] LUNG-HAN PENG[4] AND AZZEDINE BOUDRIOUA[2]

[1] *Laboratoire d'Etudes des Matériaux (LEM), Université de Jijel, 18000 Alegria*
[2] *Laboratoire de Physique de Lasers CNRS UMR 7538, Université Paris 13, Sorbonne Paris Cité, 93430 Villetaneuse, France*
[3] *Université de Lorraine, Laboratoire MatÃľriaux Optiques, Photoniques et Systèmes, EA 4423, Metz, France*
[4] *Graduate Institute of Photonics and Optoelectronics and Department of Electrical Engineering, National Taiwan University, Taipei, Taiwan*
[*] *min.lee@univ-paris13.fr*

Abstract: We have demonstrated multi-wavelength generation in a nonlinear photonic crystals of lithium tantalate. The optical parametric generation leads to second harmonic generation, sum-frequency generation and other frequency conversion in a cascade process. These conversions are assisted by all the optical nonlinear process involving $\chi^{(2)}$ and achieved by satisfying the quasi-phase matching conditions.

OCIS codes: (190.4410) Nonlinear optics, parametric processes, (190.7220) Upconversion.

References and links

1. V. Berger, "Nonlinear Photonic Crystals," Phys. Rev. Lett. **81**, 4136–4139 (1998).
2. A. Arie, N. Habshoosh, and A. Bahabad, "Quasi phase matching in two-dimensional nonlinear photonic crystals," Opt. Quant. Electron. **39**, 361–375 (2007).
3. N. G. R. Broderick, G. W. Ross, H. L. Offerhaus, D. J. Richardson, and D. C. Hanna, "Hexagonally Poled Lithium Niobate: A Two-Dimensional Nonlinear Photonic Crystal," Phys. Rev. Lett. **84**, 4345–4348 (2000).
4. L.-H. Peng and C.-C. Hsu, "Wavelength tunability of second-harmonic generation from two-dimensional $\chi^{(2)}$ nonlinear photonic crystals with a tetragonal lattice structure," Appl. Phys. Lett. **84**, 3250–3252 (2004).
5. P. Xu, J. F. Wang, C. Li, Z. D. Xie, X. J. Lv, H. Y. Leng, J. S. Zhao, and S. N. Zhu, "Simultaneous optical parametric oscillation and intracavity second-harmonic generation based on a hexagonally poled lithium tantalate," Opt. Express **17**, 4289–4294 (2009).
6. Q. Ripault, M. W. Lee, F. MÃľriche, T. Touam, B. Courtois, E. Ntsoenzok, L.-H. Peng, A. Fischer, and A. Boudrioua, "Investigation of a planar optical waveguide in 2d PPLN using Helium implantation technique," Opt. Express **21**, 7202–7208 (2013).
7. Y. Sheng, S. M. Saltiel, and K. Koynov, "Cascaded third-harmonic generation in a single short-range-ordered nonlinear photonic crystal," Opt. Lett. **34**, 656–658 (2009).
8. W. Q. Zhang, F. Yang, and X. Li, "Double quasi phase matching for both optical parametric oscillator and difference frequency generation," Opt. Commun. **282**, 1406–1411 (2009).
9. M. Levenius, V. Pasiskevicius, and K. Gallo, "Angular degrees of freedom in twin-beam parametric down-conversion," Appl. Phys. Lett. **101**, 121114 (2012).
10. M. Lazoul, A. Boudrioua, L. M. Simohamed, A. Fischer, and L.-H. Peng, "Experimental study of multiwavelength parametric generation in a two-dimensional periodically poled lithium tantalate crystal," Opt. Lett. **38**, 3892–3894 (2013).
11. L. Chen, P. Xu, Y. F. Bai, X. W. Luo, M. L. Zhong, M. Dai, M. H. Lu, and S. N. Zhu, "Concurrent optical parametric down-conversion in $\chi^{(2)}$ nonlinear photonic crystals," Opt. Express **22**, 13164–13169 (2014).
12. S. Carrasco, A. V. Sergienko, B. E. A. Saleh, M. C. Teich, J. P. Torres, and L. Torner, "Spectral engineering of entangled two-photon states," Phys. Rev. A **73**, 063802 (2006).
13. S. Witte and K. S. E. Eikema, "Ultrafast Optical Parametric Chirped-Pulse Amplification," IEEE J. Sel. Top. Quantum Electron. **18**, 296–307 (2012).
14. T. Töpfer, K. P. Petrov, Y. Mine, D. Jundt, R. F. Curl, and F. K. Tittel, "Room-temperature mid-infrared laser sensor for trace gas detection," Appl. Opt. **36**, 8042–8049 (1997).

15. X. Fang, D. Wei, D. Liu, W. Zhong, R. Ni, Z. Chen, X. Hu, Y. Zhang, S. N. Zhu, and M. Xiao, "Multiple copies of orbital angular momentum states through second-harmonic generation in a two-dimensional periodically poled $LiTaO_3$ crystal," Appl. Phys. Lett. **107**, 161102 (2015).
16. C.-Q. Xu and B. Chen, "Cascaded wavelength conversions based on sum-frequency generation and difference-frequency generation," Opt. Lett. **29**, 292–294 (2004).
17. C.-M. Lai, I.-N. Hu, Y.-Y. Lai, Z.-X. Huang, L.-H. Peng, A. Boudrioua, and A.-H. Kung, "Upconversion blue laser by intracavity frequency self-doubling of periodically poled lithium tantalate parametric oscillator," Opt. Lett. **35**, 160–162 (2010).
18. M. Levenius, V. Pasiskevicius, F. Laurell, and K. Gallo, "Ultra-broadband optical parametric generation in periodically poled stoichiometric $LiTaO_3$," Opt. Express **19**, 4121–4128 (2011).
19. M. Conforti, F. Baronio, M. Levenius, and K. Gallo, "Broadband parametric processes in $\chi^{(2)}$ nonlinear photonic crystals," Opt. Lett. **39**, 3457–3460 (2014).
20. M. Levenius, V. Pasiskevicius, and K. Gallo, "Cascaded up-conversion of twin-beam OPG in nonlinear photonic crystals," in "2013 Conference on Lasers Electro-Optics Europe International Quantum Electronics Conference CLEO EUROPE/IQEC," (2013), pp. 1–1.
21. A. Bruner, D. Eger, M. B. Oron, P. Blau, M. Katz, and S. Ruschin, "Temperature-dependent Sellmeier equation for the refractive index of stoichiometric lithium tantalate," Opt. Lett. **28**, 194–196 (2003).

Nonlinear photonic crystals have attracted great attention over decades for optical frequency conversion. They are nonlinear crystals with a 2 dimensional periodically-poled lattice such as periodically-poled lithium tantalite (2D-PPLT) and periodically-poled lithium niobate (2D-PPLN). They have a great flexibility of quasi-phase matching thank to the reciprocal lattice vectors [1] [2]. Such characteristics facilitates frequency conversion such as second harmonic generation (SHG) [3–6], sum-frequency generation (SFG) [7], difference frequency generation (DFG) [8] or optical parametric generation (OPG) [9–11]. The reciprocal lattice vectors also allow wavelength tuneability by changing temperature [4] or incident angle [9, 10].

In fact, optical frequency conversion is essential in a number of potential applications. Particularly, frequency conversion using quasi-phase matching (QPM) allows entangled photon-pair generation for quantum optics [12], amplification of ultra-fast pulses [13], gas detection sensing [14] and multiple copies of orbital angular momentum states [15].

However, the aforementioned nonlinear processes do not usually occur at the same time because of the different phase matching conditions for each process. It has been reported that SFG and DFG can be generated in a PPLN when facilitated by a cascaded process [16]. For nonlinear photonic crystals, a blue light can be generated from an OPG-signal in a SHG process using a PPLT with a square lattice [17] or a PPLT with a hexagonal lattice [5]. In some studies, it has been demonstrated that a broadband wavelength can be generated in a hexagonal nonlinear photonic crystal [18, 19]. Moreover, several nonlinear processes have been involved in multi-wavelength generation in a hexagonally-poled $LiTaO_3$ [20]. In this case, SHG and OPG were generated and SFG was then generated by a cascaded process.

In this work, we demonstrate for the first time multi-wavelength generation in a square lattice 2D PPLT exploiting multi optical nonlinear process. By pumping the crystal at 532 nm, OPG firstly occurs and OPG triggers SHG and SFG. In a single crystal, it has also been observed simultaneously three different OPG processes.

The nonlinear crystal used in this work is a lithium tantalate ($LiTaO_3$) with a thickness of 0.5 mm. The crystal is periodically poled to invert the polarisation in 2 directions as shown in Fig. 1(a). The average lattice period is $\Lambda_x = \Lambda_y = 8.52$ µm with a filling factor of 38 % in a **single set of square array**. The poled area is 2 cm×1 cm. Note that these parameters have been chosen from previous work as they allow efficient optical parametric generation with a maximum conversion efficiency [10].

Our 2D PPLT is characterised using an experimental setup illustrated in Fig. 1(b). The pump laser used in this work is a pulsed laser at 532 nm and delivers a maximum energy of 40 µJ with a pulse width of 500 ps. A half-wave plate is used to adjust the polarisation of the pump beam and a lens of 20cm focal length is positioned to inject the pump into the crystal. The peak

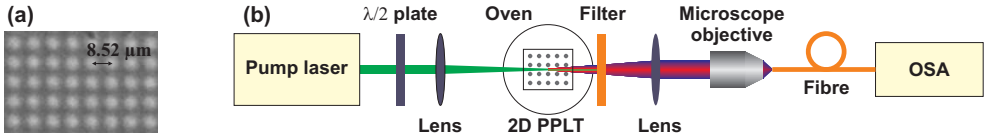

Fig. 1. (a) 2D PPLT: view on $\mathbf{Z}^+$. (b) Experimental setup. OSA: Optical Spectrum Analyser.

power can be delivered up to 80 kW which is focused to the sample with a beam waist of 95 μm, leading to a peak intensity of 282 MW/cm^2. The crystal is put in a small oven to control the crystal temperature at 110 °C. The light generated by the nonlinear process is collimated by a lens and the pump beam is removed by a band stop filter at 532 nm. The filtered light is injected into a standard multimode fibre with a core diameter of 50 μm by a microscope objective. The spectrum of multi-wavelength light is registered by an optical spectrum analyser.

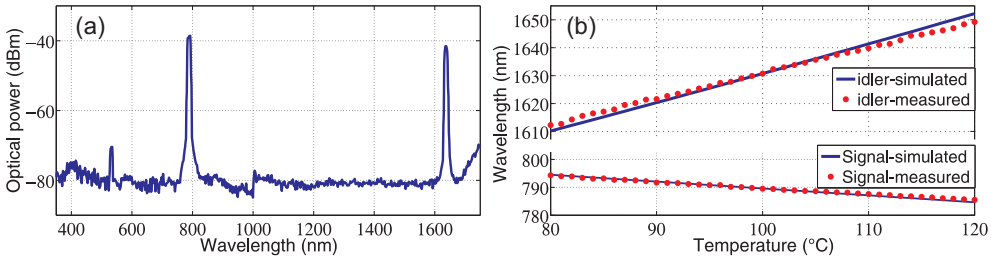

Fig. 2. (a) Spectrum with the signal (787 nm) and idler (1640 nm) measured with a peak power of 16 kW. (b) Wavelength tuneability of the signal and idler vs. temperature.

First, OPG is undertaken at a peak power of 16 kW (8 μJ) at 110 °C and an incident angle of 0 °. Figure 2(a) shows an OPG spectrum which is measured in the colinear direction with the pump source. In the figure, the peak at 532 nm is the residual pump and the peaks at 787 nm and 1640 nm are expected to be the signal and idler, respectively. These wavelengths satisfy the energy and momentum conservation laws as described in the OPG process, which are given by:

$$\frac{1}{\lambda_p} - \frac{1}{\lambda_s} - \frac{1}{\lambda_i} = 0 \tag{1}$$

$$\frac{n_p(\lambda_p, T)}{\lambda_p} - \frac{n_s(\lambda_s, T)}{\lambda_s} - \frac{n_i(\lambda_i, T)}{\lambda_i} - \frac{\sqrt{m^2 + n^2}}{\Lambda} = 0 \tag{2}$$

where $n(\lambda, T)$ is the refractive index at given wavelength λ and temperature T, m and n are the QPM orders for the reciprocal lattice vector $\mathbf{K}_{m,n}$ and Λ is the QPM period. The refractive index of Lithium Tantalate is obtained from Ref. [21]. As the measurements are undertaken in a collinear direction, 1D QPM condition can rather be considered i.e. $\mathbf{K}_{1,0}$ as a first approximation. It is found from the equations that the signal and idler occur at 787 nm and 1640 nm for a QPM period of 8.51 μm in a very good agreement with the experimental data.

This result is further emphasised by analysing the variation of the OPG interaction with the crystal temperature varied from 80 °C to 120 °C. The temperature variation results in tuning the wavelengths as shown in Fig. 2(b). The lower and upper solid lines represent the signal and idler wavelengths, respectively, obtained in simulations with a QPM period of 8.51 μm as a function of the temperature. The lower and upper circle dots indicate those measured in the experiment. It is clearly seen from the figure that the measured wavelengths for the signal and idler are again in a good agreement with those obtained in simulation. As such, this comparison confirms the assumption of 1D QPM OPG interaction with the crystal period of 8.52 μm.

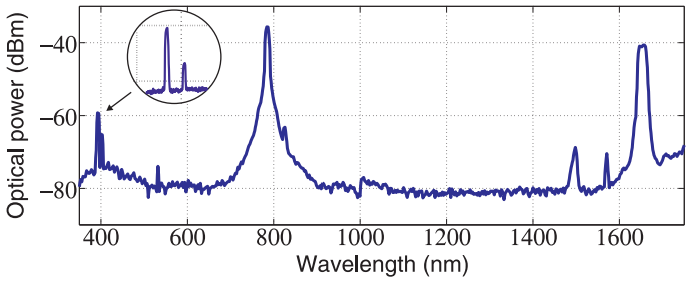

Fig. 3. Full spectrum measured at a peak power of 40 kW with a resolution of 5 nm from 350 nm to 1750 nm at 110 °C. The inset is a zoom-in spectrum around 400 nm.

In the following experiments, the peak power of the pump is increased to 40 kW (energy of 20 μJ) and the crystal temperature is set to 110 °C. Under these conditions, unexpected phenomena occur. First, a strong blue light is observed at the output of the sample. Second, as displayed in Fig. 3, the spectrum measured at this pump power from 350 nm to 1750 nm with a resolution of 5 nm shows unexpectedly another 5 peaks observed at: 393 nm, 402 nm, 820 nm, 1514 nm and 1574 nm. The signal at 787 nm and the idler at 1640 nm are present with a strong power and the other peaks are much smaller than the signal and idler. Note that these wavelengths are measured via zoom-in spectra with a resolution of 1 nm which are not presented in this paper.

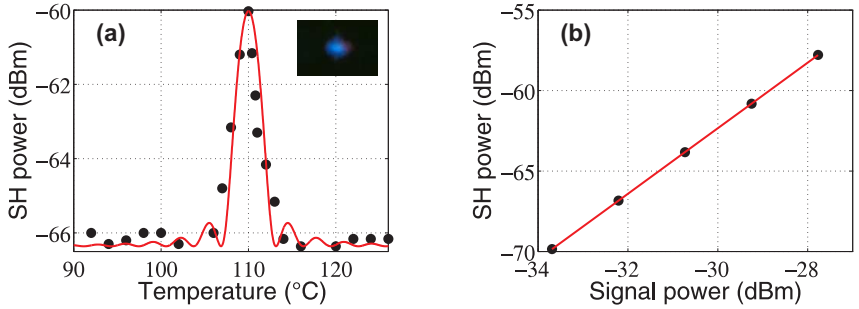

Fig. 4. **(a) SH power vs sample temperature and an image of the blue light. (b) SH power vs signal power in Log scale (dBm).**

Let us first study the peak generated at 393 nm. It is found that the wavelength of this peak is almost half of that of the signal. Therefore, it is suggested that the strong signal of 787 nm leads to SHG at 393 nm in a cascade process. In fact, the blue light observed in the work is due to the fluorescence of a paper screen by the ultraviolet light at 393 nm [the picture in Fig. 4(a)]. From the conservation equations [Eqs. (1), (2)] a SHG process is obtained when $m = 3$ and a grating period $\Lambda = 8.4$ μm which is close to 8.52 μm of our sample period. This indicates that the third order QPM ($m = 3$) contributes to the SHG in this case.

The SH power tunability is also investigated as increasing the temperature as shown in Fig. 4(a). The obtained results are fitted by using a *sinc* function. **Figure. 4(b) is the plot of the SH power versus the signal power and a linear fit in a Log scale with a slope of 2.04 which very close to 2 in theory**. These results emphasise the SHG process.

The wavelength tuneability as a function of temperature is also studied. In Fig. 5, the blue solid line is obtained by dividing the simulated signal wavelengths by 2 as in a SHG process whilst the circle dots indicate the ones measured from spectra. The measurement manifests a good agreement with the SHG simulation and the line slope is negative as in Fig. 2(b). It is shown that the SHG follows the behaviour of the signal wave obtained from the OPG process. Again,

this statement confirms a cascaded SHG process to generate the peak at 393 nm.

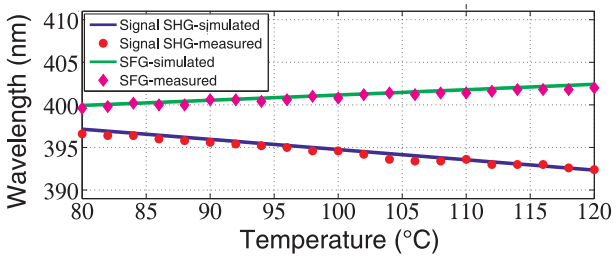

Fig. 5. Wavelength tuning as a function of the temperature for SHG and the SFG processes.

It is clearly seen from the inset of Fig. 3 that the SHG component at 393 nm is accompanied by another peak at 402 nm. It is suggested that this peak is generated by interacting the pump (532 nm) and idler (1640 nm). In this case, the two frequencies of the pump and idler are summed up in a SFG process to generate a wavelength of 402 nm. The QPM period is obtained as $\Lambda = 8.1$ µm with $m = 2$. It is therefore expected that the second order QPM contributes to this SFG process. In Fig. 5, the green solid line indicates the SFG calculated from the pump and simulated idler, and the diamond dots represent the one measured in the experiment. In the figure, the peak at 402 nm follows the same temperature dependent behaviour as the idler one as the pump wavelength remains constant. This confirms the cascaded SFG process.

We will now investigate the three remained peaks: 820 nm, 1514 nm and 1574 nm. It is worth noting from Fig. 3 that at this high pump energy the signal/idler spectrum width (i.e. gain spectrum width) of the original OPG peaks widens with the increase of pump energy, indicating an increase of the parametric gain spectrum.

At first, it is suggested from Eq. (1) that the peak at 820 nm is generated from the idler (1640 nm) in a SHG process, the peak at 1514 nm from the signal (787 nm) and idler (1640 nm) in a DFG process and the peak at 1574 nm from the signal in a parametric frequency down-conversion process for wavelength doubling. However, from Eq. (2) the QPM period is obtained as around $\Lambda = 21$ µm for these processes, which is much greater than the crystal period.

In another approach, it is found from Eqs. (1) and (2) that two other OPG processes can be responsible for these peaks. For instance, the sum of the frequencies of 820 nm and 1514 nm leads to that of the pump at 532 nm. For this process, the QPM is met with a period of 8.38 µm, which is close to the crystal period. Therefore, it is assumed that another second OPG process is involved for these wavelengths with 820 nm for signal and 1514 nm for idler. It can be, also, suggested that the pump is involved in a third OPG process with 803 nm for signal and 1574 nm for idler. In this case, the QPM period is calculated to 8.4 µm which is very close to that of the sample. It is speculated that the peak at 803 nm is present in the spectrum, but drowned in the large signal linewidth in Fig. 3. The QPM is met in the given temperature range.

As summarized in table 1, the pair of 820 nm and 1514 nm forms the second OPG process whilst the pair of 803 nm and 1574 nm is the third OPG interaction. Note that the peak at 803 nm does not appear in Fig. 3 because of the large linewidth of the signal at 787 nm.

By using the conservation equations at 110 °C, it is demonstrated that these OPG processes are a QPM interactions with $m = 1$ ($\mathbf{K}_{1,0}$) and a grating period roughly similar to the value of 8.5 µm (see table 1). In fact, the QPM interactions have been investigated for the three OPG at different temperatures. The study reveals that the QPM is satisfied with a grating period of around 8.5 µm with a QPM order of 1 ($\mathbf{K}_{1,0}$) in the range of 80 °C – 120 °C. Note that all the nonlinear interactions previously reported fulfil the energy conservation law. However, only the three OPG processes satisfy the momentum conservation law. **One possible reason for these processes with the different periods may be because of the non-uniform poling structure.**

Table 1. QPM features of cascaded nonlinear interactions in 2D-PPLT where refractive index may change with the pump intensity, leading to effective change in the QPM periodicity and then giving rise to additional OPG processes 2 and 3.

λ (nm)	interaction	QPM Λ (μm)	QPM order m
393	SHG	8.4	3
402	SFG	8.1	2
787, 1640	OPG 1	8.51	1
820, 1514	OPG 2	8.38	1
803, 1574	OPG 3	8.42	1

It is also suggested that the unexpected two OPG-like processes may assist the SHG for 820 nm, the DFG for 1514 nm and the down-conversion for 1577 nm. Therefore, one can speculate that these non-linear interactions seem to arise simultaneously in a cascaded and even mixed processes which give the observed behaviour.

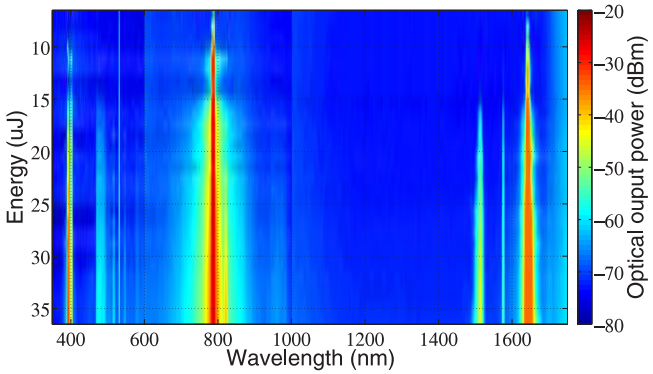

Fig. 6. Energy map from 7 μJ (49 MW/cm^2) to 37 μJ (261 MW/cm^2).

For further investigation, the pump power is varied from 7 μJ to 37 μJ at 110 °C and the spectra are measured with a step of 1 μJ as shown in Fig. 6. As seen in the figure, the SHG peak at 393 nm starts to appear clearly at 10 μJ (70 MW/cm^2). The so-called second and third OPG processes occur at 15 μJ (106 MW/cm^2).

For the first time, we have demonstrated the generation of multi-wavelength via different second order optical nonlinear process using 2D PPLT with a square lattice period of 8.52 μm. The nonlinear processes involved in the multiwavelength generation are optical parametric generation, second-harmonic generation and sum-frequency generation. The wavelengths are generated by satisfying the quasi-phase matching condition with reciprocal lattice vectors. A thorough investigation is under progress in order to completely map the nonlinear processes related to the pump parameters (angle, temperature). We are currently investigating the cause of refractive index change with the increase of pump power and **the non-colinear reciprocal vectors**, which results will be reported in a forthcoming publication.

Acknowledgements

This works has been supported by the PICS project from the CNRS and the BQR-2016 programme from the university.